



HAL
open science

Generic Stress Rectification in Nonlinear Elastic Media

Félix Benoist, Guglielmo Saggiorato, Martin Lenz

► **To cite this version:**

Félix Benoist, Guglielmo Saggiorato, Martin Lenz. Generic Stress Rectification in Nonlinear Elastic Media. *Soft Matter*, 2023, 19, pp.2970-2976. 10.1039/d2sm01606k . hal-03805460

HAL Id: hal-03805460

<https://hal.science/hal-03805460>

Submitted on 7 Oct 2022

HAL is a multi-disciplinary open access archive for the deposit and dissemination of scientific research documents, whether they are published or not. The documents may come from teaching and research institutions in France or abroad, or from public or private research centers.

L'archive ouverte pluridisciplinaire **HAL**, est destinée au dépôt et à la diffusion de documents scientifiques de niveau recherche, publiés ou non, émanant des établissements d'enseignement et de recherche français ou étrangers, des laboratoires publics ou privés.

Generic Stress Rectification in Nonlinear Elastic Media

Félix Benoist,¹ Guglielmo Saggiorato,¹ and Martin Lenz^{1,2,*}

¹Université Paris-Saclay, CNRS, LPTMS, 91400, Orsay, France[†]

²PMMH, CNRS, ESPCI Paris, PSL University,
Sorbonne Université, Université de Paris, F-75005, Paris, France

Stress propagation in nonlinear media is crucial in cell biology, where molecular motors exert anisotropic force dipoles on the fibrous cytoskeleton. While the force dipoles can be either contractile or expansile, a medium made of fibers which buckle under compression rectifies these stresses towards a biologically crucial contraction. A general understanding of this rectification phenomenon as a function of the medium's elasticity is however lacking. Here we use theoretical continuum elasticity to show that rectification is actually a very general effect in nonlinear materials subjected to anisotropic internal stresses. We analytically show that both bucklable and constitutively linear materials subjected to geometrical nonlinearities rectify small forces towards contraction, while granular-like materials rectify towards expansion. Using simulations, we moreover show that these results extend to larger forces. Beyond fiber networks, these results could shed light on the propagation of stresses in brittle or granular materials following a local plastic rearrangement.

PACS numbers: 46.35.+z, 87.16.Ln, 45.70.-n, 46.15.Ff

The active, stress-generating role of many biological materials stems from their ability to transmit internally generated forces. In cells, the action of molecular motors and the growth of protein fibers over a few nanometers generates anisotropic forces that are further transmitted by a fibrous network, the cytoskeleton, to the scale of the whole cell [1, 2]. At larger length scales, polarized cells in connective tissues exert anisotropic stresses on another fibrous network, the extracellular matrix, which again propagates these stresses far from their application point [3, 4].

The well-characterized nonlinear stress response of these networks [5–7] plays a crucial role in force transmission, allowing for the enhancement of contractile stresses [8–11] and promoting long-range mechano-sensitivity [12–16]. Beyond this quantitative stress amplification, the nonlinear response of fiber networks also leads to qualitative changes in the propagated stresses, as previously shown in numerical simulations [9]. In these simulations, a localized active unit exerts anisotropic forces in the center of a large network of discrete fibers, each of which can buckle under a sufficiently large compressive force. For localized forces much larger than this buckling threshold, the far-field stresses transmitted by the network become contractile. This is valid even in cases where the local forces are predominantly expansile, because the network resists and therefore propagates tension more than compression. This stress “rectification” has strong implications for biological force propagation, and could be one of the reasons why the actomyosin cytoskeleton is overwhelmingly observed to contract irrespective of its detailed internal architecture.

Here, we generalize these results beyond bucklable fiber networks, and demonstrate that stress rectification is a generic corollary of stress propagation in a nonlinear elastic medium. Our approach is based on a continuum formalism that allows a general discussion of arbitrary

nonlinearities. We consider both geometrical nonlinearities and generic material-dependent nonlinearities describing the response of the material to compression or tension. Nonlinearities whereby the material stiffens under tension and softens under compression are characteristic of bucklable fiber networks [6]. Conversely, materials that soften under tension and stiffen under compression, or “anti-buckle”, may offer a description of granular media, where contacts between grains are disrupted as the confining pressure is decreased [17]. Under shear, these materials experience localized plastic events known as shear transformations which generate anisotropic internal stresses similar to those induced by molecular motors in the cytoskeleton [18]. We show that the elastic constants describing the weakly nonlinear response of these materials are a reliable predictor of the sign and magnitude of rectification.

We consider a piece of homogeneous, isotropic elastic medium of dimension d comprised in a domain Ω . A set of anisotropic “active units” (*e.g.*, molecular motors or shear transformation zones) exerts forces and/or imposes local displacements on the medium. This induces a force density \mathbf{f} , resulting in a Cauchy stress tensor $\boldsymbol{\sigma}$ given by the force balance equation $f_i = -\partial\sigma_{ij}/\partial X_j$. Here $\mathbf{X} = \mathbf{x} + \mathbf{u}$ is the final location (in the “target space”) of a material point initially located in \mathbf{x} (in the “initial space”), \mathbf{u} denotes the displacement vector and the summation over repeated indices is implied. The boundary $\partial\Omega$ of the medium is held fixed, such that the forces exerted by the active units are transmitted through the medium and cause it to exert a coarse-grained stress

$$\bar{\sigma}_{ij}^a = \frac{1}{V} \oint_{\partial\Omega} \sigma_{ik} X_j dA_k \quad (1)$$

onto the boundary [19], where V is the volume of the medium and $d\mathbf{A}$ the outward-directed area element in

the target space. In the context of active matter, $\bar{\sigma}^a$ is known as the active stress generated by the overall system comprised by the medium and the active units [20]. We define as contraction (expansion) a situation where the active pressure $P_a = -\bar{\sigma}_{ii}^a/d$ is negative (positive). To investigate the relationship between the local forces \mathbf{f} and the active stress $\bar{\sigma}^a$, we define the coarse-grained local stress

$$\bar{\sigma}_{ij}^l = -\frac{1}{V} \int_{\Omega} f_i X_j dV, \quad (2)$$

where dV is the volume element in the target space. In the special case where the force transmission is entirely linear, this relation simply reads $\bar{\sigma}^a = \bar{\sigma}^l$, implying in particular an equality of the active and local pressures $P_a = P_l = -\bar{\sigma}_{ii}^l/d$. In that case, contractile (expansile) local forces always imply a contractile (expansile) active stress. These equalities are however violated in nonlinear media [19, 21], and the local and active pressures P_l and P_a can have opposite signs. We show here that this stress rectification may arise from geometrical and/or constitutive nonlinearities in the material's elastic response, and that geometrical nonlinearities always bias the system towards contraction. We then investigate the effect of generic, lowest-order constitutive nonlinearities, and characterize the regimes conducive to rectification towards contraction and expansion. Finally, we use finite-element simulations to show that our conclusions remain qualitatively valid at higher orders.

We describe the elastic deformation of our medium using the displacement gradient $\eta_{ij} = \partial u_i / \partial x_j$ and introduce the Green-Lagrange strain tensor $\boldsymbol{\varepsilon} = (\boldsymbol{\eta} + \boldsymbol{\eta}^T + \boldsymbol{\eta}^T \boldsymbol{\eta})/2$ [22]. The last, nonlinear term of $\boldsymbol{\varepsilon}$ is purely geometrical and accounts for, *e.g.*, material rotations. We express the Cauchy stress as a function of the elastic energy density E in the initial space by $\boldsymbol{\sigma} = (\mathbf{1} + \boldsymbol{\eta}) \frac{\partial E}{\partial \boldsymbol{\varepsilon}} (\mathbf{1} + \boldsymbol{\eta}^T) / \det(\mathbf{1} + \boldsymbol{\eta})$, where $\mathbf{1}$ denotes the unit tensor. We first consider a constitutively linear material with a quadratic energy density $E = \kappa \varepsilon_{ii}^2/2 + \mu(\varepsilon_{ij}^2 - \varepsilon_{ii}^2/d)$, where κ and μ are the bulk and shear moduli. We use the divergence theorem to turn the right-hand side of Eq. (1) into a volume integral, and combine the expression of the Cauchy stress, the force balance equation and Eq. (2) to find

$$P_a = P_l - \int_{\Omega} \frac{dv}{Vd} \left[\frac{\kappa}{2} (d\eta_{ij}^2 + 4\varepsilon_{ii}^2) + 4\mu(\varepsilon_{ij}^2 - \varepsilon_{ii}^2/d) \right] \leq P_l, \quad (3)$$

where the integral runs over the initial space. The inequality in Eq. (3) is proven in the SI and means that the system as a whole is always more contractile than the local forces, implying that geometrical nonlinearities always induce a rectification towards contraction.

To describe nonlinearities resulting from the medium's constitutive properties, we consider a two-dimensional

isotropic, achiral elastic medium with a non-harmonic energy density:

$$E = \frac{\kappa + \kappa' \varepsilon_{ii}/3}{2} \varepsilon_{ii}^2 + \frac{\mu + \mu' \varepsilon_{ii}}{d} (d\varepsilon_{ij}^2 - \varepsilon_{ii}^2) + \mathcal{O}(\eta^4), \quad (4)$$

where the coefficients κ' , μ' can be of either sign and characterize the most general, lowest-order nonlinearity. According to Eq. (4), when the material is isotropically dilated by a relative amount $\varepsilon_{ii} \sim \delta V/V_0$ its bulk (shear) modulus exceeds that of a purely harmonic material by $\kappa' \delta V/V_0$ ($\mu' \delta V/V_0$). More generally, we may consider a combination of bulk expansion and simple shear

$$\boldsymbol{\eta} = \begin{pmatrix} \eta_{ii}/2 & \eta_{xy} \\ 0 & \eta_{ii}/2 \end{pmatrix}, \quad (5)$$

compute the Cauchy stress tensor, and derive the differential bulk and shear moduli as

$$K = \frac{\partial \sigma_{xx}}{\partial \eta_{ii}} = \kappa (1 + \kappa_1 \eta_{ii}) + \mathcal{O}(\eta^2), \quad (6a)$$

$$G = \frac{\partial \sigma_{xy}}{\partial \eta_{xy}} = \mu (1 + \mu_1 \eta_{ii}) + \mathcal{O}(\eta^2), \quad (6b)$$

where the first order nonlinear corrections to the moduli $\kappa_1 = 1/2 + \kappa'/\kappa$ and $\mu_1 = \kappa/\mu + 1/2 + \mu'/\mu$ include contributions from geometrical as well as constitutive nonlinearities. Based on rheology measurements, we estimate $\kappa_1 \approx 100$ and $\mu_1 \approx 30$ for gels of the extracellular matrix filaments fibrin and collagen [23]. These positive values are consistent with the notion that biological fiber networks buckle, and therefore soften, under compression ($\eta_{ii} < 0$). Conversely, granular materials tend to increase their cohesion under compression. Experiments and simulations on polydisperse soft spheres near jamming thus suggest $\kappa_1 \approx 0$ and $\mu_1 \in [-400, -4]$ (see Refs. [24, 25] and SI). An intermediate behavior is observed in fiber networks with stiff grain-like inclusions mimicking connective tissues. This gives rise to a more complicated sign combination which depends on the inclusion density [26, 27]. Finally, a standard ("neo-Hookean") model of rubber displays $\kappa_1 > 0$ and $\mu_1 < 0$ with small values [28, 29], see SI.

To explicitly predict the active pressure resulting from rectification, we consider a simple circular piece of elastic medium with radius r_{out} and a single active unit at its center. The active unit is a circle with radius r_{in} at rest, and undergoes a radial displacement [Fig. 1(a)]

$$\mathbf{u}(r_{\text{in}}) = r_{\text{in}} [e_0 + e_2 \cos(2\theta)] \hat{\mathbf{r}}. \quad (7)$$

This induces a mixture of compression, tension and shear on the medium. Symmetry imposes that the local and active stress tensors take the form

$$\bar{\boldsymbol{\sigma}}^x = - \begin{pmatrix} P_x + S_x & 0 \\ 0 & P_x - S_x \end{pmatrix}, \quad (8)$$

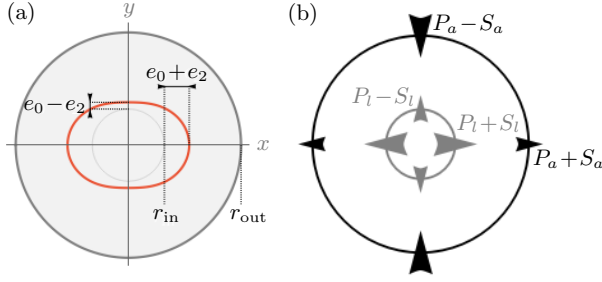


FIG. 1. Sketches of the imposed anisotropic displacement and the resulting coarse-grained stresses. (a) In the target configuration, the inner light-gray circle with radius r_{in} is moved to the orange ring. (b) Stress components in a particular situation where the local pressure P_l is positive and the active pressure P_a at the boundary is negative.

in Cartesian coordinates, for $x \in \{l, a\}$ [Fig. 1(b)]. As shown in Eq. (2), the local coarse-grained stress $\bar{\sigma}^l$ is the ratio of a force dipole by the volume V . Assuming a constant local dipole, $\bar{\sigma}^l$ thus decreases with increasing system size V due to dilution. A similar statement holds for $\bar{\sigma}^a$. It is thus useful for our discussion to define the quantities $\mathcal{P}_x = P_x(r_{\text{out}}/r_{\text{in}})^2$ and $\mathcal{S}_x = S_x(r_{\text{out}}/r_{\text{in}})^2$ which are not subject to this dilution. In this sense, they behave as force dipole components. In the following, we consider the lowest order in the weakly nonlinear regime $e_0, e_2 \ll 1$ (see SI). We perturbatively solve the force balance equation using Eq. (7) as well as the fixed boundary condition in r_{out} to compute the pressure and shear components $\mathcal{P}_x, \mathcal{S}_x$ as

$$\mathcal{P}_x = A_x e_0 + B_x e_2^2 + \mathcal{O}(e_0^2, e_0 e_2^2, e_2^4), \quad (9a)$$

$$\mathcal{S}_x = C_x e_2 + \mathcal{O}(e_2 e_0, e_2^3), \quad (9b)$$

where the cumbersome dependence of A_x, B_x and C_x on the properties of the medium is detailed in the SI. The active stresses can then be computed from the local ones through

$$\mathcal{P}_a \sim \mathcal{P}_l + \alpha \mathcal{S}_l^2, \quad \mathcal{S}_a \sim \mathcal{S}_l. \quad (10)$$

Here $\alpha\mu$ is a dimensionless function of $r_{\text{out}}/r_{\text{in}}, \kappa/\mu, \kappa_1$ and μ_1 that is obtained by combining A_x, B_x and C_x . At this order in nonlinearity, stress propagation in a medium with $\alpha = 0$ resembles that in a linear medium (namely $\mathcal{P}_a = \mathcal{P}_l, \mathcal{S}_a = \mathcal{S}_l$). Conversely, a medium with a negative (positive) α harnesses the anisotropy of the active unit to produce an additional medium-wide contraction (expansion). Equation (10) is formally valid for local stresses much smaller than the elastic moduli of the medium ($\mathcal{P}_l, \mathcal{S}_l \ll \kappa$, where “ κ ” stands for the typical magnitude of the linear moduli). It implies that when $\sqrt{\kappa} \mathcal{P}_l \ll \mathcal{S}_l$, the sign of the active pressure induced by a highly anisotropic active unit is determined not by the

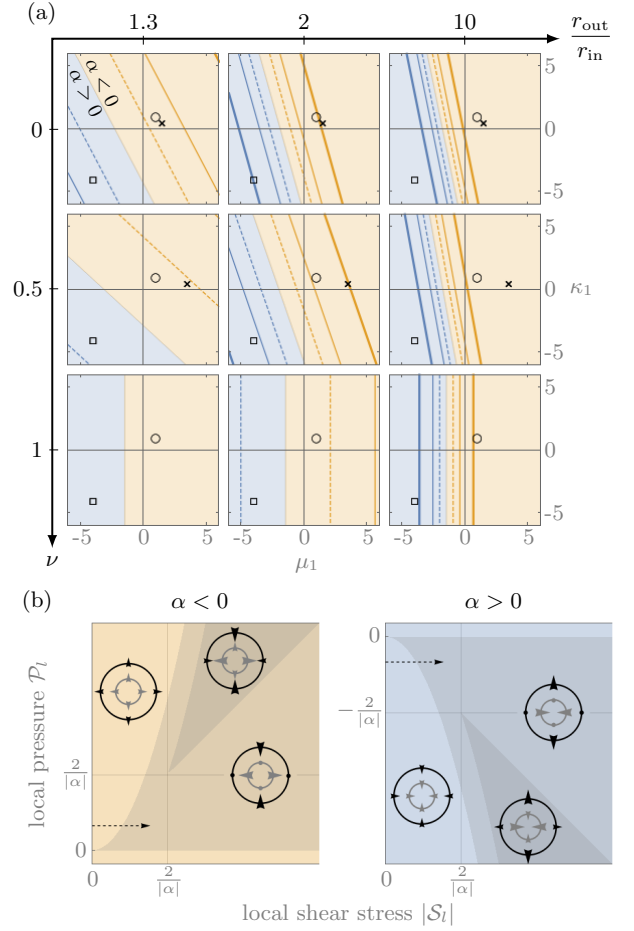


FIG. 2. Bucklable materials ($\kappa_1, \mu_1 > 0$) rectify towards contraction (yellow), while very anti-bucklable materials ($\kappa_1, \mu_1 < -3/2$) rectify towards expansion (blue). (a) Contour plot of α , indicating the overall sign of rectification as a function of the relative system size $r_{\text{out}}/r_{\text{in}}$, the Poisson ratio ν ($\nu = 1$ denotes incompressibility in 2D) and the nonlinear corrections to the moduli κ_1, μ_1 . The contour lines denote $|\alpha|\mu = 2$ (thick), 1 (thin), 0.5 (dashed). Crosses indicate constitutively linear materials where only geometrical nonlinearities are present (for $\nu = 1$ they are far to the right). Circles and squares point out specific media discussed in Fig. 3. (b) Dependence of the signs of the components of the active stress (dark arrows in the insets) as functions of the local stress components. Regions without shading correspond to situations where the signs are the same as in the absence of rectification. In regions with intermediate shading ($|\mathcal{P}_l| \lesssim |\alpha|\mathcal{S}_l^2$), the sign of \mathcal{P}_a is reversed. In the dark regions, $|\mathcal{P}_l|$ and $|\mathcal{S}_l|$ are so large that all components of $\bar{\sigma}_a$ (dark regions) are reversed [SI]. These changes of signs are illustrated by arrows in the small pictures. Some arrows are replaced by circles in the intermediate shading regime to indicate that they are smaller than the other arrows and can point either way.

values ($\mathcal{P}_l, \mathcal{S}_l$) characterizing the active unit, but by the properties of the medium through the sign of α .

We illustrate the influence of the material's properties on the sign of α in Fig. 2(a), which indicates a clear tendency of fiber-like (granular-like) materials towards contractile (expansile) rectification. Indeed, when κ_1 and μ_1 are both larger (smaller) than a critical value of $-3/2$, the system always rectifies towards contraction (expansion). As a result, a material with $\kappa_1 = \mu_1 = 0$ is contractile because of the contractile character of geometrical nonlinearities described by Eq. (3). Media with $\kappa_1 > -3/2$ but $\mu_1 < -3/2$ or the reverse can be either contractile or expansile depending on the system size $r_{\text{out}}/r_{\text{in}}$ and Poisson's ratio $\nu = (\kappa - \mu)/(\kappa + \mu)$. Finally, $|\alpha|$ increases with increasing r_{out} such that $|\alpha(\infty) - \alpha(r_{\text{out}})| \propto (r_{\text{in}}/r_{\text{out}})^2$ for large r_{out} (see SI), implying that larger systems rectify more. For example, larger fiber networks allow for more extensive buckling, resulting in stronger rectification and the coming together of the contour lines of Fig. 2(a) as r_{out} increases. Finally, Fig. 2(b) shows that for large enough local stresses, rectification can cause a sign-switching not only in the active pressure but in all components of the active stress tensor $\bar{\sigma}_a$.

While these calculations are strictly valid only for small local stresses, one may hope that Eq. (10) remains qualitatively correct for strong active units with $\mathcal{P}_l \approx \mathcal{S}_l \gtrsim \kappa$. We test this expectation through finite element simulations [SI] of a fully (*i.e.*, not weakly) nonlinear model with an elastic energy density

$$E = \frac{\kappa}{2} \frac{(J-1)^2}{1+a(J-1)} + \frac{\mu}{2} \frac{I/J-2}{1+b(J-1)}, \quad (11)$$

where $J = \det(\mathbf{1} + \boldsymbol{\eta})$, $I = \text{Tr}(\mathbf{1} + 2\boldsymbol{\varepsilon})$ and the constants a, b are defined through $\kappa_1 = 1/2 - 3a$, $\mu_1 = -3/2 - b$. The case $a = b = 0$ corresponds to a compressible neo-Hookean model for rubber elasticity. We illustrate a bucklable and an anti-bucklable material in Fig. 3 by choosing two media with $\kappa_1 = \mu_1 = -4$ and $\kappa_1 = \mu_1 = 1$ (equidistant from $-3/2$, as denoted by symbols in Fig. 2(a)). As expected, the former induces contraction while the latter causes expansion. The quantitative predictions of Eq. (10) moreover remain largely valid up to local stress values comparable with the bulk modulus of the network, which implies deformations of the medium of order one. These conclusions also hold in other parameter regimes and for a model specifically designed to mimic the shear-stiffening behavior of fiber networks (Fig. S4) [5]. In addition, simulations of isotropic active units with large local stress values suggest that rectification effects also manifest in that case (Fig. S5) [9].

Our intuition of the mechanics of nonlinear materials is largely based on deforming their outer boundary. We thus expect a uniformly compressed material to respond with an expansile stress, while applying shear will elicit an opposing shear stress. In this study, we show that if the forces are exerted from the *inside* of the material, these expectations can be upset. In the most extreme cases,

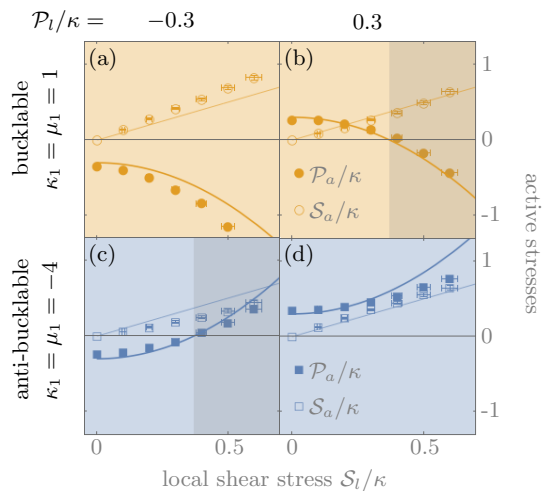


FIG. 3. The small-stress asymptotic prediction of Eq. (10) (lines) accurately capture the finite-element simulation results (symbols) even for intermediate stress values. Here $\nu = 0.1$ and $r_{\text{out}}/r_{\text{in}} = 2$ in the geometry of Fig. 1. (a,b) A fiber-like bucklable model, (c,d) a very anti-bucklable model mimicking a granular medium. The values of \mathcal{P}_l , \mathcal{S}_l pictured in (b,c) are marked by dashed arrows in Fig. 2(b), and background shading follows the same convention. The error bars denote the estimated magnitude of the error induced by the finiteness of the simulation mesh size.

an embedded active unit that expands (contracts) in all directions can elicit contractile (expansile) stresses in all directions. The system thus “forgets” the shape of the active units, and its large-scale behavior is controlled by the characteristics of the elastic material instead. Expansion- and shear-stiffening (softening) materials thus always rectify towards contraction (expansion). This rectification tends to be stronger in more compressible materials and in larger systems. These behaviors arise in a continuum model with or without constitutive nonlinearities, and are thus generic in elastic media beyond previously studied discrete fiber networks.

While most of our calculations are conducted in a circular 2D system with a single active unit, they are likely to remain valid in more complex settings provided the elastic medium is homogeneous. Indeed, Refs. [9, 19] show that if an active unit is far enough away from the boundary of the medium and from other active units, its contribution to the total active stress is independent of the characteristics of either. This remains true as long as the distance between active units is larger than the distance over which each of them induces significant nonlinear deformations. In our small-strain formalism (which also describes intermediate strains well), this distance is of the order of $r^* \sim 10 r_{\text{in}}$ [SI].

In the strongly nonlinear regime, rectification in fiber networks is strikingly similar to the results of our weakly nonlinear formalism [9], which may explain why acto-

myosin networks are always contractile despite the presence of mixed force dipoles [30, 31]. Its application to discrete granular media and other amorphous solids remains to be investigated. Experiments do however suggest that the elastic response of a foam to a shear transformation zone becomes more isotropic in the vicinity of the jamming transition [32], where nonlinear effects are expected to play a large role. We speculate that such effects could be explained by the type of rectification described here. They could then significantly affect the characteristics of the yielding transition in nearly-jammed systems [33, 34].

We thank Pierre Ronceray and Mehdi Bouzid for many discussions and suggestions, and Lev Truskinovsky for comments on the manuscript. ML was supported by Marie Curie Integration Grant PCIG12-GA-2012-334053, “Investissements d’Avenir” LabEx PALM (ANR-10-LABX-0039-PALM), ANR grants ANR-15-CE13-0004-03 and ANR-21-CE11-0004-02, as well as ERC Starting Grant 677532. ML’s group belongs to the CNRS consortium AQV.

* martin.lenz@universite-paris-saclay.fr

† felix.benoist@lptms.u-psud.fr

- [1] J. Howard, *Mechanics of Motor Proteins and the Cytoskeleton* (Sinauer Associates, 2001).
- [2] L. Blanchoin, R. Boujemaa-Paterski, C. Sykes, and J. Plastino, *Physiological Reviews* **94**, 235 (2014).
- [3] U. S. Schwarz and S. A. Safran, *Rev. Mod. Phys.* **85**, 1327 (2013).
- [4] S. A. Maskarinec, C. Franck, D. A. Tirrell, and G. Ravichandran, *Proceedings of the National Academy of Sciences* **106**, 22108 (2009).
- [5] M. L. Gardel, J. H. Shin, F. C. MacKintosh, L. Mahadevan, P. Matsudaira, and D. A. Weitz, *Science* **304**, 1301 (2004).
- [6] C. Storm, J. J. Pastore, F. C. MacKintosh, T. C. Lubensky, and P. A. Janmey, *Nature* **435**, 191 (2005).
- [7] O. Chaudhuri, S. H. Parekh, and D. A. Fletcher, *Nature* **445**, 295 (2007).
- [8] M. P. Murrell and M. L. Gardel, *Proceedings of the National Academy of Sciences* **109**, 20820 (2012),.
- [9] P. Ronceray, C. P. Broedersz, and M. Lenz, *Proceedings of the National Academy of Sciences* **113**, 2827 (2016).
- [10] P. Ronceray, C. P. Broedersz, and M. Lenz, *Soft Matter* **15**, 331 (2019).
- [11] Y. L. Han, P. Ronceray, G. Xu, A. Malandrino, R. D. Kamm, M. Lenz, C. P. Broedersz, and M. Guo, *Proc. Natl. Acad. Sci. U.S.A.* **10.1073/pnas.1722619115** (2018).
- [12] P. Rosakis, J. Notbohm, and G. Ravichandran, *Journal of the Mechanics and Physics of Solids* **85**, 16 (2015).
- [13] J. Notbohm, A. Lesman, P. Rosakis, D. A. Tirrell, and G. Ravichandran, *Journal of The Royal Society Interface* **12**, 20150320 (2015).
- [14] X. Xu and S. A. Safran, *Physical Review E* **92**, 032728 (2015).
- [15] H. Wang, A. Abhilash, C. S. Chen, R. G. Wells, and V. B. Shenoy, *Biophysical Journal* **107**, 2592 (2014).
- [16] R. S. Sopher, H. Tokash, S. Natan, M. Sharabi, O. Shelah, O. Tchaicheyan, and A. Lesman, *Biophysical journal* , **1802.05075** (2018).
- [17] W. G. Ellenbroek, M. van Hecke, and W. van Saarloos, *Phys. Rev. E* **80**, 061307 (2009).
- [18] A. Amon, V. B. Nguyen, A. Bruand, J. Crassous, and E. Clément, *Phys. Rev. Lett.* **108**, 135502 (2012).
- [19] P. Ronceray and M. Lenz, *Soft Matter* **11**, 1597 (2015).
- [20] J. Prost, F. Jülicher, and J.-F. Joanny, *Nat. Phys.* **11**, 111 (2015).
- [21] A. E. Carlsson, *Physical Review E* **74**, 051912 (2006).
- [22] P. Wriggers, *Nonlinear Finite Element Methods*, 1st ed. (Springer, Berlin, Heidelberg, 2008).
- [23] A. S. G. van Oosten, M. Vahabi, A. J. Licup, A. Sharma, P. A. Galie, F. C. MacKintosh, and P. A. Janmey, *Scientific Reports* **6**, 19270 (2016).
- [24] C. S. O’Hern, L. E. Silbert, A. J. Liu, and S. R. Nagel, *Phys. Rev. E* **68**, 011306 (2003).
- [25] M. van Hecke, *Journal of Physics: Condensed Matter* **22**, 033101 (2009).
- [26] J. L. Shivers, J. Feng, A. S. G. van Oosten, H. Levine, P. A. Janmey, and F. C. MacKintosh, *Proceedings of the National Academy of Sciences* **117**, 21037 (2020).
- [27] A. S. G. van Oosten, X. Chen, L. Chin, K. Cruz, A. E. Patteson, K. Pogoda, V. B. Shenoy, and P. A. Janmey, *Nature* **573**, 96 (2019).
- [28] L. R. G. Treloar, *Reports on Progress in Physics* **36**, 755 (1973).
- [29] Y. Shokef and S. A. Safran, *Physical Review Letters* **108**, 178103 (2012).
- [30] S. Hatano, *Int. Rev. Cytology* **156**, 199 (1994).
- [31] M. Lenz, M. L. Gardel, and A. R. Dinner, *New Journal of Physics* **14**, 033037 (2012).
- [32] K. W. Desmond and E. R. Weeks, *Phys. Rev. Lett.* **115**, 098302 (2015).
- [33] A. Nicolas, E. E. Ferrero, K. Martens, and J.-L. Barrat, *Rev. Mod. Phys.* **90**, 045006 (2018).
- [34] S. Merabia and F. Detcheverry, *EPL (Europhysics Letters)* **116**, 46003 (2016).

Supporting information for “Generic stress rectification in nonlinear elastic media”

I. CONSTITUTIVELY LINEAR MEDIA RECTIFY TOWARDS CONTRACTION

In this section, we consider only geometrical nonlinearities and set out to prove the inequality in Eq. (3). Firstly, the elastic energy density E is written with the Green-Lagrange strain tensor $\boldsymbol{\varepsilon} = (\boldsymbol{\eta} + \boldsymbol{\eta}^\top + \boldsymbol{\eta}^\top \boldsymbol{\eta})/2$, which depends quadratically on the displacement gradient $\eta_{ij} = \partial u_i / \partial x_j$. We further define the symmetric part of the displacement gradient $U_{ij} = (\eta_{ij} + \eta_{ji})/2$ which corresponds to the linearized strain. The stress tensor which naturally derives from E describes the surface force measured in the initial space with respect to the initial area: $d\mathbf{F}^0/d\mathbf{a} = \partial E / \partial \boldsymbol{\varepsilon}$, it is known as the second Piola-Kirchhoff stress. Then in order to find the Cauchy stress measured fully in the target space: $\boldsymbol{\sigma} = d\mathbf{F}/d\mathbf{A}$, we need to transform the surface force and the area as

$$d\mathbf{F} = (\mathbf{1} + \boldsymbol{\eta}) d\mathbf{F}^0 \quad \text{and} \quad d\mathbf{a} = \frac{\mathbf{1} + \boldsymbol{\eta}^\top}{\det(\mathbf{1} + \boldsymbol{\eta})} d\mathbf{A}, \quad (\text{S1})$$

which ultimately gives the formula for the Cauchy stress in the main text [1]. Then, given the quadratic energy density $E = \kappa \varepsilon_{ii}^2 / 2 + \mu (\varepsilon_{ij}^2 - \varepsilon_{ii}^2 / d)$, the stress-strain relation displays a linear stress term $\boldsymbol{\sigma}^L$ proportional to \mathbf{U} , and a term which includes the geometrical nonlinearities $\boldsymbol{\sigma}^G$:

$$\boldsymbol{\sigma}^L = (\kappa - 2\mu/d) U_{ii} \mathbf{1} + 2\mu \mathbf{U}, \quad (\text{S2a})$$

$$\boldsymbol{\sigma}^G = (\kappa - 2\mu/d) (\eta_{ij}^2 / 2 - U_{ii}^2) \mathbf{1} + \mu (4\mathbf{U}^2 + \boldsymbol{\eta} \boldsymbol{\eta}^\top) + 2(\kappa - 2\mu/d - \mu) U_{ii} \mathbf{U} + \mathcal{O}(\eta^3). \quad (\text{S2b})$$

Secondly, given the force balance equation $f_i = -\partial \sigma_{ij} / \partial X_j$, the difference between the local and active coarse-grained stresses can be integrated by part to read

$$\bar{\sigma}^a - \bar{\sigma}^l = \frac{1}{V} \int_{\Omega} \boldsymbol{\sigma} dV = \frac{1}{V} \int_{\Omega} \boldsymbol{\sigma} \det(\mathbf{1} + \boldsymbol{\eta}) dv, \quad (\text{S3})$$

where dv is the volume element in the initial space. Equation (S3) is known as the mean stress theorem [2, 3]. Due to this relation, writing $\mathbf{S} = \boldsymbol{\sigma} \det(\mathbf{1} + \boldsymbol{\eta})$ and decomposing $\mathbf{S} = \mathbf{S}^L + \mathbf{S}^G$ as we did $\boldsymbol{\sigma}$ in Eq. (S2), the pressure difference reads $P_a - P_l = -\int S_{ii} / (Vd)$. Due to our fixed boundary condition, the integral of the trace of the linear term $\mathbf{S}^L = \boldsymbol{\sigma}^L$ vanishes and the trace of the nonlinear term is expressed in a closed form as

$$S_{ii}^G = \frac{\kappa}{2} (d\eta_{ij}^2 + 4\varepsilon_{ii}^2) + 4\mu (\varepsilon_{ij}^2 - \varepsilon_{ii}^2 / d). \quad (\text{S4})$$

Here, κ and μ are both positive for mechanical stability. Thus, for $d \geq 2$, the geometrical term S_{ii}^G always gives a positive (contractile) contribution to the active stress. Indeed, using the eigenvalues $\lambda_i \in \mathbb{R}$ of the symmetric matrix $\boldsymbol{\varepsilon}$, we can rewrite $\varepsilon_{ij}^2 - \varepsilon_{ii}^2 / d = \sum_{i < j} (\lambda_i - \lambda_j)^2 / d$, which is always non-negative. As a result S_{ii}^G is a sum of squares that is also non-negative, implying the inequality of Eq. (3): $P_a - P_l \leq 0$.

Finally, we present an alternative derivation of this relation that highlights its frame indifference. The integrand of Eq. (3) can be rewritten using the deformation gradient $\boldsymbol{\Lambda} = \mathbf{1} + \boldsymbol{\eta}$ and the right Cauchy-Green deformation tensor $\mathbf{C} = \boldsymbol{\Lambda}^\top \boldsymbol{\Lambda} = \mathbf{1} + 2\boldsymbol{\varepsilon}$. Indeed, since

$$\mathbf{S} = \boldsymbol{\Lambda} \frac{\partial E}{\partial \boldsymbol{\varepsilon}} \boldsymbol{\Lambda}^\top, \quad \text{where} \quad \frac{\partial E}{\partial \boldsymbol{\varepsilon}} = \frac{\kappa}{2} (C_{ii} - d) \mathbf{1} + \mu (\mathbf{C} - C_{ii} \mathbf{1} / d), \quad (\text{S5})$$

we can write

$$S_{ii} = \frac{\kappa}{2} [(C_{ii} - d)^2 + dC_{ii}] + \mu [C_{ij}^2 - C_{ii}^2 / d]. \quad (\text{S6})$$

We see that the right-hand side Eq. (S6) is a sum of squares plus a term $\propto C_{ii} = d + 4\eta_{ii} + 4\eta_{ij}^2$. Since η_{ii} is integrated to zero due to the fixed boundary condition, the term in Eq. (S6) also gives a contractile contribution to $P_a - P_l$.

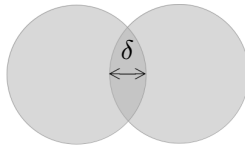


FIG. S1. Overlap between two interacting beads in a granular simulation.

II. ELASTIC MODULI IN GRANULAR MEDIA NEAR JAMMING

Here, we derive typical values of κ_1 and μ_1 for granular media near the jamming transition. Let us consider a large equilibrium packing of bidisperse frictionless spherical grains in a 2D box with volume fraction ϕ . The grains interact through a harmonic potential $\mathcal{V} \sim k \delta^2$, where k is a spring constant, and δ the overlap divided by the sum of the two bead diameters, see Fig. S1. For volume fractions slightly above the jamming transition $\phi_c \approx 0.84$, granular media display a strongly nonlinear elastic behavior. Indeed, multiple simulations and experiments [4, 5] have shown that while the bulk modulus goes to a finite limit in ϕ_c^+ and can thus be approximated by a constant, the shear modulus scales with $\phi - \phi_c$ and vanishes at the transition. This can be expressed as

$$K/k \sim A \quad \text{and} \quad G/k \sim B(\phi - \phi_c)^b, \quad \text{for } 0 < \phi - \phi_c \ll 1, \quad (\text{S7})$$

where $A, B \approx 0.2$ and $b \approx 0.5$. Based on this model, we impose an isotropic compression characterized by a displacement gradient tensor $\eta_{ij} = -\eta_0 \delta_{ij}/d$ on our granular material initially at ϕ_c , where $0 < \eta_0 \ll 1$. This results in a new volume fraction ϕ_0 such that

$$\phi_0 - \phi_c = \phi_0 \eta_0 = \phi_c \frac{\eta_0}{1 - \eta_0} > 0. \quad (\text{S8})$$

We then compute the elastic moduli κ and μ , and their nonlinear corrections κ_1 and μ_1 around this value of ϕ_0 .

Let the bulk strain $\eta_{ii} = -\eta_0 + \delta\eta$, where $|\delta\eta| \ll \eta_0$, corresponding to a volume fraction $\phi \sim \phi_0 - \phi_c \delta\eta$. Then similarly to Eq. (6), the moduli are expressed as $K \sim \kappa(1 + \kappa_1 \delta\eta)$ and $G \sim \mu(1 + \mu_1 \delta\eta)$, where the parameters are derived from Eq. (S7):

$$\begin{aligned} \kappa/k &= A, & \kappa_1 &= 0, \\ \mu/k &= B \left(\frac{\phi_c \eta_0}{1 - \eta_0} \right)^b, & \mu_1 &= -\frac{b}{\eta_0(1 - \eta_0)}. \end{aligned} \quad (\text{S9})$$

Therefore, while κ_1 vanishes, μ_1 diverges at the transition and scales as $(\phi_0 - \phi_c)^{-1}$. And close to the transition, around *e.g.* $\phi_0 - \phi_c = 0.001, 0.01$ or 0.1 , we find respectively $\mu_1 \approx -400, -40$ or -4 as in the main text.

III. COARSE-GRAINED STRESSES IN THE CIRCULAR GEOMETRY

In this section, we present the analytical calculations leading to the expressions of the coarse-grained stresses $\bar{\sigma}$ in Eq. (9) and of the rectification coefficient α of Eq. (10) of the main text. We first rewrite the coarse-grained stresses in the initial space where the calculations will be easier to handle in Sec. III A. Then in Sec. III B we present the Ansatz for the displacement field that allows us to solve the force balance condition. In Sec. III C, we show the expressions of the coarse-grained pressures and shear stresses with the stress and displacement fields. We finally display the detailed expressions of the coarse-grained stresses $\bar{\sigma}$ in the circular geometry as well as the expression of α in Sec. III D.

A. Rewriting the coarse-grained stresses in the initial space

In order to calculate the coarse-grained stresses, we need to express them in the initial configuration, where the force density $\phi = \mathbf{f}/\det(\mathbf{1} + \boldsymbol{\eta})$ is related to the first Piola-Kirchhoff stress tensor $\boldsymbol{\tau} = (\mathbf{1} + \boldsymbol{\eta}) \frac{\partial E}{\partial \boldsymbol{\epsilon}}$. The force balance equation thus reads $\phi_i = -\partial_j \tau_{ij}$ and the coarse-grained stresses can be rewritten as

$$\bar{\sigma}_{ij}^a = \frac{1}{V} \oint_{\partial\Omega} \tau_{ik} X_j da_k \quad \text{and} \quad \bar{\sigma}_{ij}^l = -\frac{1}{V} \int_{\Omega} \phi_i X_j dv, \quad (\text{S10})$$

where $\mathbf{d}\mathbf{a}$ is the outward-directed area element in the initial space. As before in Sec. I, we distinguish the linear term $\boldsymbol{\tau}^L$ (which is the same in the initial and target spaces $\boldsymbol{\tau}^L = \boldsymbol{\sigma}^L$), from the nonlinear term $\boldsymbol{\tau}^{\text{NL}} = \boldsymbol{\tau}^G + \boldsymbol{\tau}^C$. This last equality distinguishes the geometrical and constitutive nonlinearities. Given the non-harmonic energy density of Eq. (4), up to second order, the terms read

$$\boldsymbol{\tau}^L = (\kappa - 2\mu/d)U_{ii} \mathbf{1} + 2\mu \mathbf{U}, \quad (\text{S11a})$$

$$\boldsymbol{\tau}^G = (\kappa - 2\mu/d)\eta_{ij}^2 \mathbf{1}/2 + \mu \boldsymbol{\eta}^T \boldsymbol{\eta} + (\kappa - 2\mu/d)U_{ii} \boldsymbol{\eta} + 2\mu \boldsymbol{\eta} \mathbf{U} + \mathcal{O}(\eta^3). \quad (\text{S11b})$$

$$\boldsymbol{\tau}^C = 3(\kappa' - 2\mu'/d)U_{ii}^2 \mathbf{1}/2 + \mu' U_{ij}^2 \mathbf{1} + 2\mu' U_{ii} \mathbf{U} + \mathcal{O}(\eta^3). \quad (\text{S11c})$$

B. Ansatz for the displacement field

In the initial space, the material is subjected to zero body force except at r_{in} , where the stress is discontinuous. The fixed boundary at r_{out} and the imposed displacement at r_{in} additionally impose boundary conditions on the stress and displacement fields, resulting in the following system of equations:

$$\begin{cases} \nabla \cdot \boldsymbol{\tau}^T = \mathbf{0}, & \text{for } r \in [0, r_{\text{in}}) \cup (r_{\text{in}}, r_{\text{out}}) \\ \mathbf{u} = \mathbf{0}, & \text{at } r = 0 \text{ and } r = r_{\text{out}} \\ \mathbf{u} = r_{\text{in}} [e_0 + e_2 \cos(2\theta)] \hat{\mathbf{r}}, & \text{at } r = r_{\text{in}} \end{cases}. \quad (\text{S12})$$

We solve this system perturbatively by expanding $\mathbf{u}, \boldsymbol{\eta}, \boldsymbol{\tau}$ in the small scalar quantity

$$\eta \sim |e_0| + |e_2|. \quad (\text{S13})$$

The displacement gradient is hence written $\boldsymbol{\eta} = \boldsymbol{\eta}^L + \boldsymbol{\eta}^{\text{NL}} + \mathcal{O}(\eta^3)$ where the L and NL superscript refer to linear and quadratic (nonlinear) terms in η . This allows us to write the stress tensor as

$$\boldsymbol{\tau} = \boldsymbol{\tau}^L(\boldsymbol{\eta}^L) + \boldsymbol{\tau}^L(\boldsymbol{\eta}^{\text{NL}}) + \boldsymbol{\tau}^{\text{NL}}(\boldsymbol{\eta}^L) + \mathcal{O}(\eta^3), \quad (\text{S14})$$

where $\boldsymbol{\tau}^L(\boldsymbol{\eta}^L)$ is of order 1, while the next two are of order 2. The linear displacement field \mathbf{u}^L is the solution of $\partial_i \tau_{ji}^L(\boldsymbol{\eta}^L) = 0$. This is solved by decomposing \mathbf{u}^L in the following Fourier modes due to the form of the imposed displacement:

$$u_r^L/r_{\text{in}} = e_0 \alpha_0(r) + e_2 \alpha_2(r) \cos 2\theta, \quad (\text{S15a})$$

$$u_\theta^L/r_{\text{in}} = e_2 \beta_2(r) \sin 2\theta. \quad (\text{S15b})$$

Here $\alpha_0(r), \alpha_2(r), \beta_2(r)$ are sums of r^k , with $k \in \{-3, -1, 1, 3\}$ and coefficients depending on the boundary conditions. Then, at the first nonlinear order, \mathbf{u}^{NL} is the solution of the linear equation $\partial_i \tau_{ji}^{\text{NL}}(\boldsymbol{\eta}^{\text{NL}}) = -\partial_i \tau_{ji}^{\text{NL}}(\boldsymbol{\eta}^L)$ which is solved by expanding \mathbf{u}^{NL} as

$$u_r^{\text{NL}}/r_{\text{in}} = e_2^2 \gamma_0(r) + e_0 e_2 \gamma_2(r) \cos 2\theta + e_2^2 \gamma_4(r) \cos 4\theta, \quad (\text{S16a})$$

$$u_\theta^{\text{NL}}/r_{\text{in}} = e_0 e_2 \delta_2(r) \sin 2\theta + e_2^2 \delta_4(r) \sin 4\theta, \quad (\text{S16b})$$

where the $\gamma_i(r), \delta_i(r)$ are again sums of r^k with k odd between -7 and $+5$. As a consequence, we obtain in Sec. III D the strain and stress fields up to second order in η .

C. Calculations of the coarse-grained stresses

We compute the coarse-grained active stress $\bar{\boldsymbol{\sigma}}^a$ and local stress $\bar{\boldsymbol{\sigma}}^l$ in the circular geometry by integrating the stresses in the material as in Eq. (S10). The coarse-grained stresses are expressed in Cartesian coordinates, while the stress field is more easily expressed in polar coordinates. In the following (and in this subsection only), we denote Cartesian indices x, y with Greek letters (μ, ν) and polar indices r, θ with Latin letters (i, j, k) . The change-of-basis matrix between these two systems reads $\mathbf{R} = \begin{pmatrix} \cos \theta & -\sin \theta \\ \sin \theta & \cos \theta \end{pmatrix}$. In the circular geometry of Fig. 1 where the active unit

produces a discontinuity in the stress at r_{in} in the initial configuration, the coarse-grained stresses are expressed as follows:

$$\bar{\sigma}_{\mu\nu}^a = \frac{1}{\pi r_{\text{out}}^2} \oint_{\partial\Omega} R_{\mu i} \tau_{ik} R_{\nu j} X_j da_k = \frac{1}{\pi} \int_0^{2\pi} d\theta R_{\mu i} \tau_{ir}(r_{\text{out}}, \theta) R_{\nu r}, \quad (\text{S17a})$$

$$\bar{\sigma}_{\mu\nu}^l = \frac{1}{\pi r_{\text{out}}^2} \int_{\Omega} R_{\mu i} \partial_k \tau_{ik} R_{\nu j} X_j dV = \frac{1}{\pi} \frac{r_{\text{in}}^2}{r_{\text{out}}^2} \int_0^{2\pi} d\theta R_{\mu i} [\tau_{ir}(r_{\text{in}}^+, \theta) - \tau_{ir}(r_{\text{in}}^-, \theta)] R_{\nu r} \left[1 + \frac{u_r(r_{\text{in}}, \theta)}{r_{\text{in}}} \right], \quad (\text{S17b})$$

where $\partial_k \tau_{ik}$ denotes the stress divergence expressed in polar coordinates. Then, introducing $\beta = (r_{\text{out}}/r_{\text{in}})^2$, the active pressure and shear stress rescaled so as to compensate for dilution read

$$\beta(\bar{\sigma}_{xx}^a + \bar{\sigma}_{yy}^a) = -2\mathcal{P}_a = \frac{\beta}{\pi} \int \tau_{rr}(r_{\text{out}}, \theta), \quad (\text{S18a})$$

$$\beta(\bar{\sigma}_{xx}^a - \bar{\sigma}_{yy}^a) = -2\mathcal{S}_a = \frac{\beta}{\pi} \int [\tau_{rr}(r_{\text{out}}, \theta) \cos 2\theta - \tau_{\theta r}(r_{\text{out}}, \theta) \sin 2\theta], \quad (\text{S18b})$$

with similar expressions for the local pressure and shear stress:

$$-2\mathcal{P}_l = \frac{1}{\pi} \int [\tau_{rr}(r_{\text{in}}^+, \theta) - \tau_{rr}(r_{\text{in}}^-, \theta)] \left[1 + \frac{u_r(r_{\text{in}}, \theta)}{r_{\text{in}}} \right], \quad (\text{S19a})$$

$$-2\mathcal{S}_l = \frac{1}{\pi} \int \left\{ [\tau_{rr}(r_{\text{in}}^+, \theta) - \tau_{rr}(r_{\text{in}}^-, \theta)] \cos 2\theta - [\tau_{\theta r}(r_{\text{in}}^+, \theta) - \tau_{\theta r}(r_{\text{in}}^-, \theta)] \sin 2\theta \right\} \left[1 + \frac{u_r(r_{\text{in}}, \theta)}{r_{\text{in}}} \right]. \quad (\text{S19b})$$

D. Full expressions of the coarse-grained stresses

In Eqs. (9-10), we consider small displacements with two independent parameters $e_0, e_2 \ll 1$. In the weakly nonlinear formalism, the simplest possible rectification requires that the term in e_0 be similar (and of opposite sign) to the term in e_2^2 . In this regime, given $\epsilon \ll 1$, the displacement parameters read $e_0 = \epsilon \tilde{e}_0$ and $e_2 = \sqrt{\epsilon} \tilde{e}_2$. As a result $\mathcal{P}_x = \epsilon \tilde{\mathcal{P}}_x$ and $\mathcal{S}_x = \sqrt{\epsilon} \tilde{\mathcal{S}}_x$ for $x \in \{l, a\}$, where the tildes denote quantities of order one. Then to lowest order in ϵ , Eq. (9) can be rewritten as

$$\tilde{\mathcal{P}}_x = A_x \tilde{e}_0 + B_x \tilde{e}_2^2 + \mathcal{O}(\epsilon), \quad (\text{S20a})$$

$$\tilde{\mathcal{S}}_x = C_x \tilde{e}_2 + \mathcal{O}(\epsilon), \quad (\text{S20b})$$

implying that the “ \sim ” symbols of Eq. (10) denote equalities to lowest order in ϵ . The rectification behavior thus depends on the ratio $\tilde{\mathcal{P}}_l/(\alpha \tilde{\mathcal{S}}_l^2)$, *i.e.* on $\tilde{e}_0/\tilde{e}_2^2$. We further display the complete expressions of the coefficients in Eq. (9) obtained after finding the strain field through force balance (see Sec. III B) and integrating the resulting stress via Eq. (S11), as in (S18) and (S19). In order to make sense of the cumbersome expressions of the A_x, B_x and C_x , we introduce several quantities: $X = (3 - \nu)^2(1 + \beta^2) + 2(3 - 6\nu - \nu^2)\beta$,

$$\begin{aligned} a_0 &= 1215 - 1863\nu + 756\nu^2 - 126\nu^3 + 87\nu^4 - 43\nu^5 + 6\nu^6 \\ &\quad + (81 - 2457\nu + 2412\nu^2 - 594\nu^3 + 265\nu^4 + 155\nu^5 - 22\nu^6)\beta \\ &\quad + (1782 - 3798\nu + 6216\nu^2 - 3948\nu^3 + 326\nu^4 - 286\nu^5 + 28\nu^6)\beta^2 \\ &\quad - (918 + 1170\nu - 2616\nu^2 + 1044\nu^3 + 54\nu^4 - 262\nu^5 + 12\nu^6)\beta^3 \\ &\quad + (459 + 45\nu + 132\nu^2 - 918\nu^3 + 515\nu^4 - 71\nu^5 - 2\nu^6)\beta^4 \\ &\quad - (891 - 1755\nu + 1188\nu^2 - 294\nu^3 - 13\nu^4 + 17\nu^5 - 2\nu^6)\beta^5, \end{aligned}$$

$$\begin{aligned} a_1 &= 1863 - 756\nu - 54\nu^2 + 12\nu^3 + 7\nu^4 + (1377 - 1260\nu + 102\nu^2 - 108\nu^3 - 31\nu^4)\beta \\ &\quad + (1782 - 1368\nu + 804\nu^2 + 168\nu^3 + 54\nu^4)\beta^2 + (162 - 504\nu - 132\nu^2 - 24\nu^3 - 46\nu^4)\beta^3 \\ &\quad + (243 + 108\nu + 18\nu^2 - 84\nu^3 + 19\nu^4)\beta^4 - (243 - 324\nu + 162\nu^2 - 36\nu^3 + 3\nu^4)\beta^5, \end{aligned}$$

$$\begin{aligned}
a_2 = & 2511 - 4104\nu + 4023\nu^2 - 1416\nu^3 + 173\nu^4 - 48\nu^5 + 13\nu^6 \\
& + (1377 - 8352\nu + 6369\nu^2 - 2568\nu^3 - 77\nu^4 + 104\nu^5 - 53\nu^6)\beta \\
& + (6966 - 16128\nu + 17430\nu^2 - 6480\nu^3 + 1890\nu^4 - 176\nu^5 + 82\nu^6)\beta^2 \\
& + (2754 - 9216\nu + 6162\nu^2 - 1392\nu^3 - 794\nu^4 + 240\nu^5 - 58\nu^6)\beta^3 \\
& + (2187 - 3672\nu + 3843\nu^2 - 1896\nu^3 + 545\nu^4 - 128\nu^5 + 17\nu^6)\beta^4 \\
& - (243 - 189\nu^2 + 72\nu^3 + 9\nu^4 - 8\nu^5 + \nu^6)\beta^5,
\end{aligned}$$

and

$$\begin{aligned}
b_0 = & 81 - 270\nu + 234\nu^2 - 36\nu^3 + 13\nu^4 - 6\nu^5 + (135 - 378\nu + 366\nu^2 - 196\nu^3 - 29\nu^4 + 22\nu^5)\beta \\
& + (162 - 708\nu + 1116\nu^2 - 464\nu^3 + 82\nu^4 - 28\nu^5)\beta^2 + (126 - 564\nu + 540\nu^2 - 168\nu^3 - 106\nu^4 + 12\nu^5)\beta^3 \\
& + (45 - 222\nu + 426\nu^2 - 188\nu^3 + 17\nu^4 + 2\nu^5)\beta^4 + (27 - 162\nu + 198\nu^2 - 100\nu^3 + 23\nu^4 - 2\nu^5)\beta^5,
\end{aligned}$$

$$\begin{aligned}
b_1 = & 27 - 18\nu + 3\nu^2 + (189 + 18\nu - 11\nu^2)\beta + (174 + 12\nu + 14\nu^2)\beta^2 \\
& + (138 - 12\nu - 6\nu^2)\beta^3 + (39 + 6\nu - \nu^2)\beta^4 + (9 - 6\nu + \nu^2)\beta^5,
\end{aligned}$$

$$\begin{aligned}
b_2 = & 243 - 270\nu + 84\nu^2 - 34\nu^3 + 9\nu^4 + (189 - 522\nu + 404\nu^2 + 58\nu^3 - 33\nu^4)\beta \\
& + (510 - 1356\nu + 568\nu^2 - 84\nu^3 + 42\nu^4)\beta^2 + (474 - 612\nu + 312\nu^2 + 100\nu^3 - 18\nu^4)\beta^3 \\
& + (159 - 486\nu + 244\nu^2 - 10\nu^3 - 3\nu^4)\beta^4 + (153 - 210\nu + 116\nu^2 - 30\nu^3 + 3\nu^4)\beta^5.
\end{aligned}$$

In the end, we find

$$A_l = A_a = \frac{4\kappa\beta}{(1+\nu)(\beta-1)}, \quad (\text{S21a})$$

$$B_l = -\kappa\beta \frac{(3-\nu)a_0 + (1-\nu)^2(1+\nu)a_1\kappa_1 + (1-\nu)a_2\mu_1}{(3-\nu)^2(1+\nu)(\beta-1)^2X^2}, \quad (\text{S21b})$$

$$B_a = -\kappa\beta \frac{b_0 + (1-\nu)^2(1+\nu)b_1\kappa_1 + (1-\nu)b_2\mu_1}{(1+\nu)(\beta-1)^2X^2}, \quad (\text{S21c})$$

$$C_l = C_a = 4\mu\beta \frac{2(3+\nu) + (3-\nu)(\beta+\beta^2)}{(\beta-1)X}. \quad (\text{S21d})$$

As expected from the linear elasticity analysis of Sec. I, the coefficients in front of the linear e_0 and e_2 terms are identical for the local and boundary stresses, but discrepancies appear in the e_2^2 terms. This leads us to define $\alpha = (B_a - B_l)/C_l^2$.

IV. BEHAVIOR OF α AND RECTIFICATION SATURATION RADIUS r^*

To help better understand the lengthy expression of the rectification coefficient $\alpha = (B_a - B_l)/C_l^2$ in subsection III.D, we hereby discuss its dependence on the system size r_{out} . As is apparent from Fig. 2(a), α increases with increasing r_{out} for relatively small systems, then saturates as the size of the system goes to infinity. Indeed, away from the high-stress region close to the active unit, the stress decrease causes the nonlinearities to become negligible in front of the linear terms. Therefore, we examine the radius r^* at which stress propagation switches from nonlinear to linear. To this end we define the system size parameter $\beta = (r_{\text{out}}/r_{\text{in}})^2$. In the limit $\beta \rightarrow \infty$, Eq. (S21) leads to $\alpha(\beta) = \alpha_\infty + \alpha_1/\beta + \mathcal{O}(\beta^{-2})$, where

$$\begin{aligned}
\mu\alpha_\infty = & -\frac{(\kappa_1 + \frac{3}{2})(1-\nu^2) + (\mu_1 + \frac{3}{2})(5-2\nu+\nu^2)}{4}, \\
\mu\alpha_1 = & \frac{(\kappa_1 + \frac{3}{2})(15-6\nu-8\nu^2+6\nu^3-7\nu^4) + (\mu_1 + \frac{3}{2})(111-36\nu+50\nu^2-20\nu^3+7\nu^4)}{4(3-\nu)^2}.
\end{aligned} \quad (\text{S22})$$

We introduce the value of the parameter β such that α is within 10% of its large-size limit through $\left| \frac{\alpha(\beta_{10}) - \alpha_\infty}{\alpha_\infty} \right| = 0.1$. The square-root of β_{10} , corresponding to the ratio of the radii, lies between 4 and 9, except for insignificant values

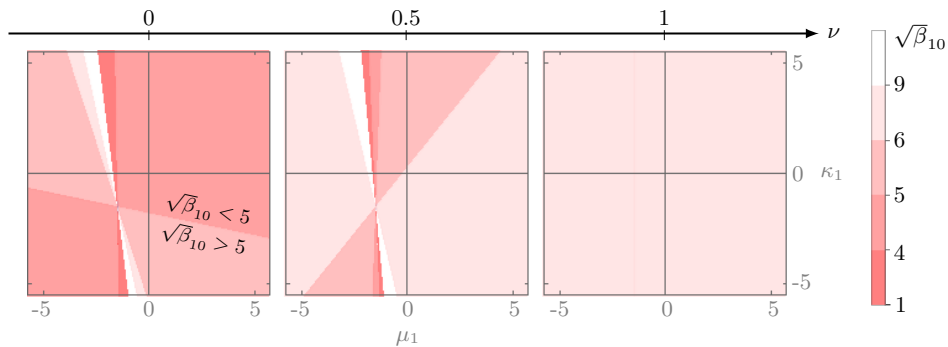


FIG. S2. The rectification saturation radius r^* is generally of the order of r_{in} . Contour plot of $\sqrt{\beta_{10}} = r^*/r_{\text{in}}$ when κ_1 and μ_1 are varied for several values of Poisson's ratio ν . Except in the small white regions, $\sqrt{\beta_{10}} < 9$. In these white regions, $|\alpha|$ tends to take negligible values.

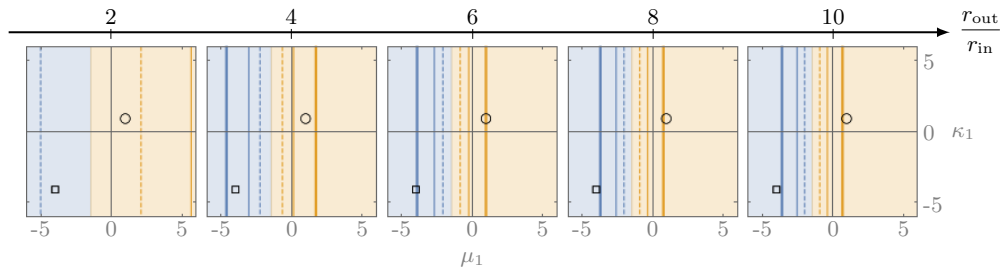


FIG. S3. Rectification happens mostly near the active unit. Additional plots to Fig. 2(a) showing the stabilization of the graphs as the system size increases for a Poisson's ratio $\nu = 1$. The blue and yellow lines at constant $|\alpha|\mu$ stay quite still between $r_{\text{out}}/r_{\text{in}} = 8$ and 10 . The behavior is similar for $\nu = 0$.

of α , see Fig. S2. Fig. S3 also illustrates this behavior by showing the stabilization of the lines at constant α as the system size increase. Therefore, defining the rectification saturation radius r^* such that $\beta_{10} = (r^*/r_{\text{in}})^2$, increasing r_{out} past $r^* \sim 10r_{\text{in}}$ has little influence on the value of $\mathcal{P}_a - \mathcal{P}_l$, *i.e.* on the rectification effect. This indicates that the propagation is nonlinear only up to r^* . In the study of stress propagation from multiple active units, one thus needs to compare this r^* to the typical spacing between two active units.

V. THE RECTIFICATION DIAGRAM

Let us give further explanation to the shadings of the rectification diagram of Fig. 2(b), corresponding to different rectification regimes. In the circular geometry of Fig. 1, provided that α and \mathcal{P}_l have different signs, a change of sign of \mathcal{P}_a due to rectification can appear for all values of the local pressure \mathcal{P}_l as long as the local shear stress $|\mathcal{S}_l|$ is large enough. Indeed, in Eq. (10) the sign switching of the active pressure \mathcal{P}_a (*e.g.* $\mathcal{P}_a < 0$ while $\mathcal{P}_l > 0$) requires

$$|\alpha|\mathcal{S}_l^2 \gtrsim |\mathcal{P}_l|. \quad (\text{S23})$$

This sets the boundary between the regions with light shading and the regions with intermediate shading. Then, the extreme case where all active stress components switch sign (*e.g.* $\mathcal{P}_a \pm \mathcal{S}_a < 0$ while $\mathcal{P}_l \pm \mathcal{S}_l > 0$) happens for

$$|\mathcal{S}_l| \lesssim |\mathcal{P}_l| \lesssim |\alpha|\mathcal{S}_l^2 - |\mathcal{S}_l|, \quad (\text{S24})$$

i.e. for $|\mathcal{P}_l|$ and $|\mathcal{S}_l|$ both larger than $2/|\alpha|$. This extreme case corresponds to the dark regions of Fig. 2(b).

VI. FINITE-ELEMENT SIMULATIONS

This section provides further details on the finite element simulations used to produce Fig. 3 of the main text. Sec. VIA describes our simulation methods. In Sec. VIB, we discuss rectification in two additional fully nonlinear models.

A. Methods

We solve the set of equations (S12) via simulations with the finite element software Fenics [6] version 2019.2.0.dev0. We use a mesh with maximal size $l = 0.01$ for $r_{\text{in}} = 1$ and $r_{\text{out}} = 2$, and another one with $l = 0.1$ for $r_{\text{out}} = 10$. They were both created with Gmsh version 4.4.1. In all figures, the error bars correspond to the differences between two meshes at l and $l/10$, which gives roughly 5% of S_l or \mathcal{P}_l for all points. The meshes are created without enforcing rotational symmetry, which results in small non-zero values for the non-diagonal coefficients that should be zero in a continuum system (*e.g.*, $\bar{\sigma}_{xy}^l$), as shown in Eq. (8). However, we find that these values are smaller than 5% of the diagonal coefficients in all simulations. In the geometry of Fig. 1, if we apply too large a deformation at r_{in} , we come into contact with the fixed boundary at r_{out} , which poses some numerical issues. Therefore, we can only perform accurate simulations up to about $\eta = |e_0| + |e_2| \sim 0.6$.

B. Additional data

In the main text, we studied two models with clear buckling and anti-buckling behaviors, which lead to a readily observable reversal of the active pressure sign, due to rectification. Here, we study two other models where these behaviors are less pronounced: a standard neo-Hookean model of rubber, and another one which can mimic the shear-stiffening behavior of fiber networks. Consistent with analytical predictions, these systems display a smaller propensity for rectification, and we show that the predictions of Eq. (10) remain valid up to intermediate stress values.

In the fully nonlinear model with the elastic energy density of Eq. (11), we introduced the parameters a, b such that $\kappa_1 = 1/2 - 3a$ and $\mu_1 = -3/2 - b$. In Fig. 3, we showed the good agreement between the weakly nonlinear predictions of Eq. (10) and finite-element simulations for the bucklable and anti-bucklable models obtained by setting $(a, b) = (-1/6, -5/2)$ and $(3/2, 5/2)$ to obtain $(\kappa_1, \mu_1) = (1, 1)$ and $(-4, -4)$ respectively. We now consider the neo-Hookean model, obtained by setting $a = b = 0$ in Eq. (11). It has $\kappa_1 = 1/2$, $\mu_1 = -3/2$ and we recover the predicted small tendency to rectify towards contraction, see Fig. S4(a,b).

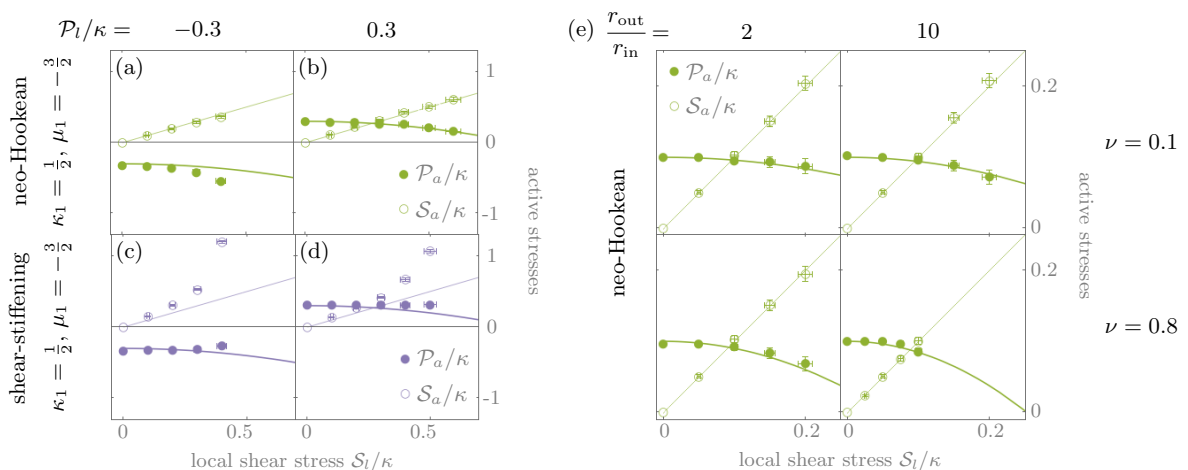


FIG. S4. Additional plots of the coarse-grained stresses are in agreement with Eq. (10) up to intermediate stresses and in a large scale of parameters. (a-b) Rubber-like neo-Hookean model [$a = b = 0$ in Eq. (11)]. (c-d) Fiber-like shear-stiffening model of Eq. (S25) with $c = 10$, following the predictions up to the point where stresses diverge (when $\eta \sim 1/\sqrt{c}$). For all plots, $\nu = 0.1$ and $r_{\text{out}}/r_{\text{in}} = 2$. (e) For $\mathcal{P}_l = 0.1\kappa$, the predictions at $\nu = 0.8$ and $r_{\text{out}}/r_{\text{in}} = 10$ remain quantitatively accurate.

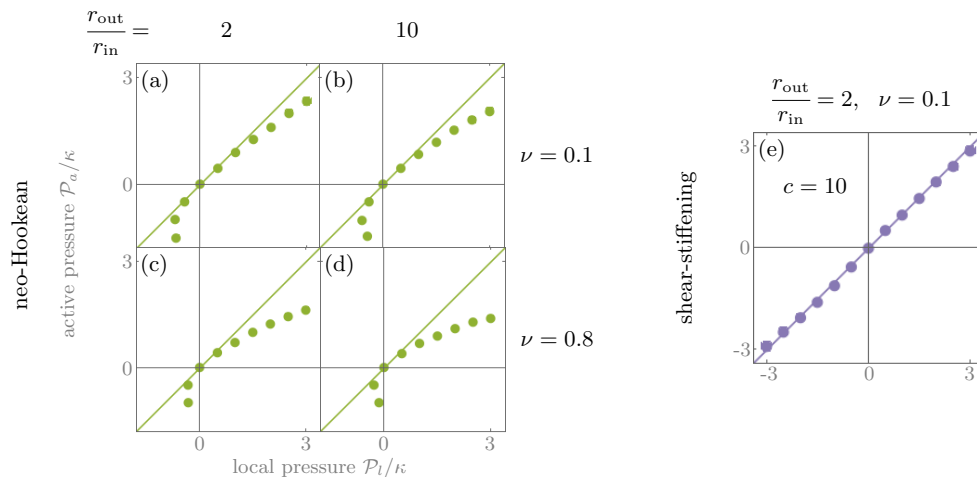


FIG. S5. Investigation of the $\mathcal{P}_a \sim \mathcal{P}_l$ relationship of Eq. (10) for $\mathcal{S}_l = 0$. The predictions at zero shear stress (*i.e.* $|\mathcal{S}_l|, |\mathcal{S}_a| < 0.01\kappa$) remain reasonably accurate up to a few \mathcal{P}_l/κ . (a-d) In the neo-Hookean case, the nonlinear terms are such that $\mathcal{P}_a < \mathcal{P}_l$ and become increasingly significant as ν and $r_{\text{out}}/r_{\text{in}}$ increase. Specifically, the agreement deteriorates from panel (a) to panels (b) and (c), to panel (d). (e) In the shear-stiffening case these nonlinear terms are first decreased up to $c \sim 2-5$ [see Eq. (S25)] and then increased in the opposite direction (such that $\mathcal{P}_a > \mathcal{P}_l$).

We then investigate a variant of the neo-Hookean model which has the shear-stiffening behavior $G \propto \sigma_{xy}^{3/2}$ characteristic of fiber networks under large strains. Its elastic energy density reads [7, 8]

$$E = \frac{\kappa}{2} (J - 1)^2 + \frac{\mu}{2c} \left[1 - c(I/J - 2) \right]^{-1}, \quad (\text{S25})$$

where $J = \det(\mathbf{1} + \boldsymbol{\eta})$ and $I = \text{Tr}(\mathbf{1} + 2\boldsymbol{\varepsilon})$. Here, the shear strain threshold for the stiffening behavior corresponds to a fraction of $1/\sqrt{c}$, the strain at which the shear stress diverges. This is such that the neo-Hookean model is recovered for $c = 0$. This model still has $\kappa_1 = 1/2$, $\mu_1 = -3/2$, which corresponds to the same tendency to rectify towards contraction as in the neo-Hookean case. Indeed, c only affects higher order nonlinearities. As shown in Fig. S4(c,d) where $c = 10$, we recover Eq. (10) at small stress. But due to the shear stress divergence at finite shear strain in Eq. (S25), our predictions fail when $\mathcal{S}_l/\kappa \gtrsim 1/\sqrt{c}$. Furthermore, the agreement between the simulations with the neo-Hookean model and Eq. (10) remains quantitative in the small stress regime for all considered values of the Poisson's ratio ν and the ratio of the boundary radius to the active unit radius $r_{\text{out}}/r_{\text{in}}$, see Fig. S4(e).

We finally compare the dependence of \mathcal{P}_a with \mathcal{P}_l at zero shear stress with the weakly nonlinear prediction $\mathcal{P}_a \sim \mathcal{P}_l$. As displayed in Fig. S5, we recover the prediction for small stresses, but higher order nonlinearities induce significant deviations for \mathcal{P}_l/κ outside of $[-0.3, 1]$. In the end, we see that the predictions of Eq. (10) relating the active and local stress components fail when either the local pressure or the local shear stress become comparable to the bulk modulus κ . Our weakly nonlinear predictions additionally fail close to stress divergences, *i.e.* when the nonlinearities become too significant compared to the linear terms.

-
- [1] P. Wriggers, *Nonlinear Finite Element Methods*, 1st ed. (Springer, Berlin, Heidelberg, 2008).
 - [2] P. Ronceray and M. Lenz, *Soft Matter* **11**, 1597 (2015).
 - [3] A. E. Carlsson, *Physical Review E* **74**, 051912 (2006).
 - [4] C. S. O'Hern, L. E. Silbert, A. J. Liu, and S. R. Nagel, *Phys. Rev. E* **68**, 011306 (2003).
 - [5] M. van Hecke, *Journal of Physics: Condensed Matter* **22**, 033101 (2009).
 - [6] M. S. Alnæs, J. Blechta, J. Hake, A. Johansson, B. Kehlet, A. Logg, C. Richardson, J. Ring, M. E. Rognes, and G. N. Wells, *Archive of Numerical Software* **3** (2015).
 - [7] Y. Shokef and S. A. Safran, *Physical Review Letters* **108**, 178103 (2012).
 - [8] J. K. Knowles, *International Journal of Fracture* **13**, 611 (1977).